DOI: 10.1002/eqe.3654

RESEARCH ARTICLE

Probabilistic characterization of the directionality of horizontal earthquake response spectra

Alan Poulos | Eduardo Miranda

Department of Civil and Environmental Engineering, Stanford University, Stanford, CA, USA

Correspondence
Alan Poulos, Department of Civil and Environmental Engineering, Stanford University, CA 94305, USA.
Email: apoulos@stanford.edu

Summary

Earthquake response spectral ordinates vary significantly with changes in orientation within the horizontal plane. This variation is characterized probabilistically in this study using a large database of recorded earthquake ground motions. For each ground motion record, response spectral ordinates are computed in all horizontal orientations as a function of the rotation angle with respect to the azimuth of maximum response and then normalized by (1) the maximum and (2) the median spectral ordinate from all these orientations. Nonlinear regression models are then fitted to the means, standard deviations, and correlations of both ratios, as a function of rotation angle. To achieve a more complete probabilistic description, probability distributions are fitted to both ratios at each rotation angle. These results can be used for several probabilistic seismic hazard computations, such as the sampling of response spectral ordinates at specific orientations within the same site.

KEYWORDS:
ground motion, response spectra, spectral acceleration, directionality, orientation dependence

1 | INTRODUCTION

For engineering purposes, the intensity of earthquake ground motion is usually characterized by 5% damped pseudo-acceleration response spectral ordinates. Although this intensity varies significantly with changes in orientation within the horizontal plane, a phenomenon known as ground motion directionality, a single representative intensity has been used in most applications, such as in ground motion models (GMMs) and earthquake-resistant design. This scalar measure of ground motion intensity has commonly been constructed by combining the intensities in the two horizontal as-recorded sensor orientations by computing, for example, their geometric mean. However, recent studies and GMMs have favored intensities that are independent of sensor orientation [1,2]. For example, the median and maximum intensity of all horizontal orientations are known as RotD50 and RotD100, respectively [2], with the numbers referring to percentiles of the distribution. The latest GMMs tend to favor the use of RotD50 [3], whereas building codes in the United States use RotD100 [4]. Although using measures of central tendency such as RotD50 or the geometric mean of the spectral ordinates of the two as-recorded horizontal components may be adequate for earthquake-resistant design purposes if the ground motion directionality is small, its use becomes questionable if the directionality is large [5,6]. For example, in 1 s oscillators, the intensity in the orientation of maximum response is, on average, approximately 55% larger than the one occurring in the perpendicular direction [7], therefore ground motion directionality is not small and requires more attention than the one that has been given in the past.

Ground motion directionality has usually been studied to define empirical relations between different scalar definitions of horizontal intensity [8–12]. However, relatively little attention has been given to the characterization of ground motion intensity

at arbitrary orientations within the horizontal plane. Hong and Goda[13] studied ground motion directionality by examining the variation of spectral accelerations as a function of the rotation angle from the orientation in which maximum intensity occurs (i.e., the orientation where RotD100 occurs) for 5% damped single-degree-of-freedom (SDOF) systems with periods of vibration of 0.2 and 1.0 s. To compare the directionality of records with different intensities, they normalized the spectral accelerations with respect to their maximum value reached in any orientation within the horizontal plane (RotD100). They then proposed a model for the mean of this ratio as a function of the rotation angle using a database of 592 records. Moreover, they fitted a probability distribution for the specific case of orientations that are orthogonal to the direction of the maximum intensity. More recently, Shahi and Baker[10] provided mean estimates of the same ratio but normalized by RotD50 instead of by RotD100, because RotD50 is used in recent GMMs and therefore the ratio becomes more practical to combine with GMMs.

This study extends the works of Hong and Goda[13] and Shahi and Baker[10] to provide a detailed probabilistic characterization of the same ratios used by these researchers, i.e., the ratios between the 5% damped spectral accelerations at any orientation within the horizontal plane and the maximum (RotD100) or median (RotD50) intensity for periods of vibration between 0.01 and 10 s. Nonlinear regression analyses are used to develop models for the means, standard deviations, and correlations of both ratios using the NGA-West2 database, which contains records from shallow crustal earthquakes in active tectonic regions[14]. Moreover, probability distributions are fitted to both ratios for use in more advanced applications.

2 | GROUND MOTION DIRECTIONALITY

Ground motion intensity is commonly characterized by response spectral ordinates, which correspond to the peak response (maximum of the absolute value of the response) of 5% damped linear elastic single-degree-of-freedom (SDOF) oscillators. This peak response may vary significantly with changes in orientation within the horizontal plane. For example, Figure 1 shows the relative displacement trace of an SDOF oscillator with a natural period of vibration of 1 s subjected to recorded horizontal components of an example ground motion, which was recorded during the 1999 M_W 7.1 Hector Mine earthquake at the Riverside County Fairgrounds station (i.e., record #1792 from the NGA-West2 database[14]). The orientation where the maximum peak response of the oscillator occurs is known as the major response axis[13], which for this example ground motion occurs at an azimuth of 229°. The intensity at this orientation of maximum peak response is known as RotD100[2], and is denoted here as Sd_{RotD100} to indicate that it corresponds to a spectral displacement. The response history of the oscillator at each orientation is then used to compute the variation of spectral displacement with changes in orientation and are also presented in Figure 1 using a polar representation (i.e., the spectral displacement at any orientation is given by the distance to the origin). Note that the spectral displacement repeats every 180° because of the absolute value used in its computation.

To compare the directionality of different ground motions, Hong and Goda[13] studied pseudo-spectral accelerations as a function of the angle ϕ from the major response axis, $Sa(\phi)$, and normalized them by their maximum, Sa_{RotD100}, defining the ratio:

$$\eta(\phi) = \frac{Sa(\phi)}{Sa_{\mathrm{RotD100}}} = \frac{Sd(\phi)}{Sd_{\mathrm{RotD100}}} \tag{1}$$

which can also be computed using spectral displacements because both intensities only differ by a constant factor (i.e., the square of the natural frequency). Figure 2a shows the η ratios for a period of 1 s of 100 example ground motion records, which also includes the record previously shown in Figure 1. The number of ground motion records in this figure is kept relatively low on purpose in order to allow a better visualization of the variation of intensities with changes in rotation for individual records. Note that for any ground motion, there are two lines in this figure that correspond to orientations that are clockwise and counterclockwise away from the major response axis. By definition, η is always lower than or equal to 1. Moreover, the lower bound of η is $\cos(\phi)$, which corresponds to the case of a fully polarized ground motion (i.e., one where motion takes place only along a single orientation). It is interesting to note that there is significant record-to-record variability of $\eta(\phi)$ with some ground motions showing small directionality (i.e., $\eta(\phi)$ values close to 1) while a significant number show a strong directionality (i.e., $\eta(\phi)$ values close to $\cos(\phi)$ of the fully polarized case) highlighting the need for a probabilistic characterization of this aspect of earthquake ground motions.

Given a value of Sa_{RotD100}, the $\eta(\phi)$ ratios can be used to compute pseudo-spectral accelerations at any orientation ϕ. However, most of the recent GMMs use RotD50 to define their intensity instead of RotD100, and therefore seismic hazard curves for

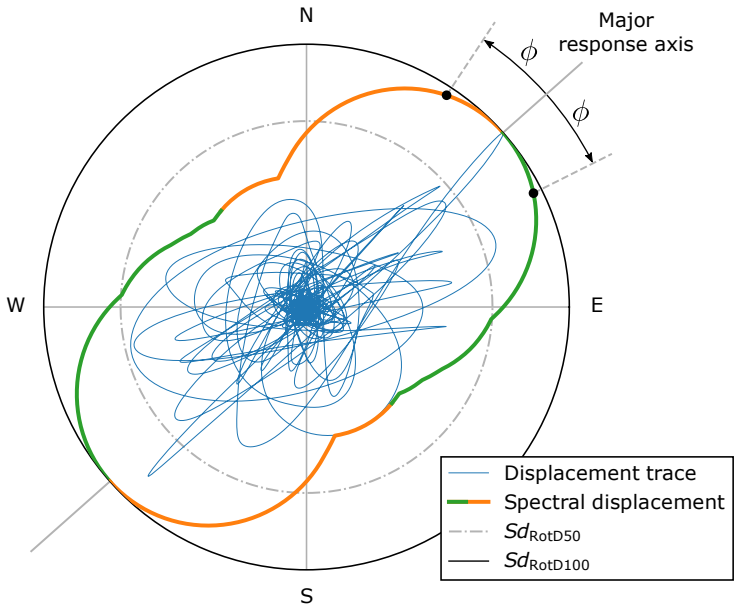

FIGURE 1 Relative displacement trace of an SDOF oscillator of period 1 s subjected to an example bidirectional horizontal ground motion record along with the variation of spectral ordinates with changes in orientation.

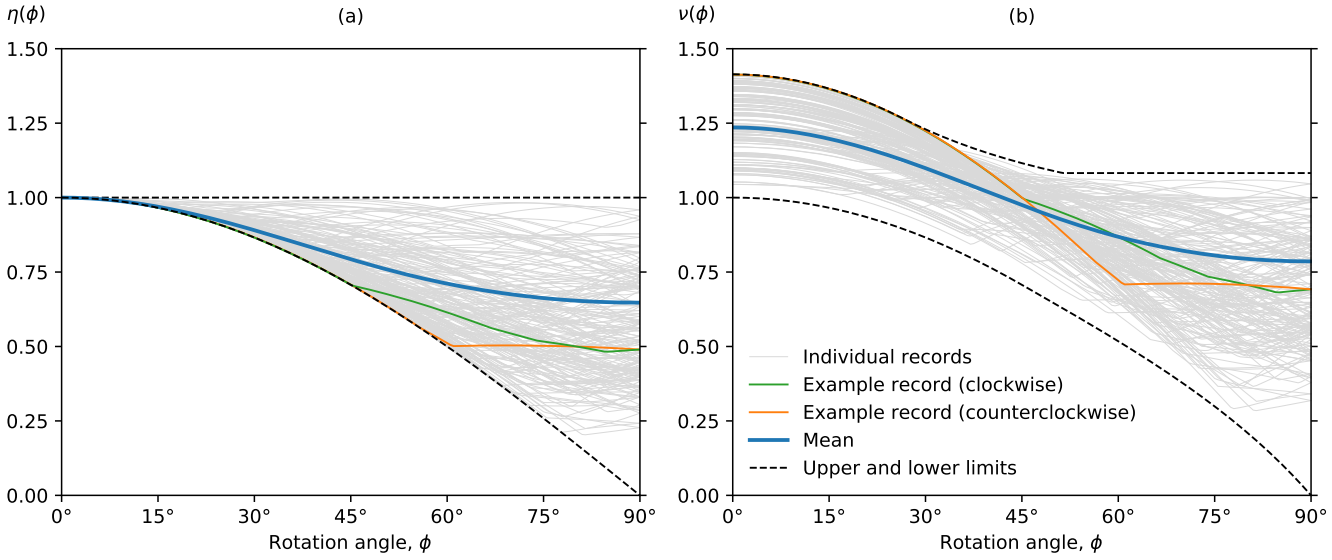

FIGURE 2 Pseudo-spectral acceleration at a rotation angle ϕ from the major response axis for an oscillator with a period of 1 s subjected to 100 recorded ground motions when normalized by (a) Sa_{RotD100} and (b) Sa_{RotD50}.

RotD100 are not readily available. Thus, this work also studies a similar ratio that is normalized by Sa_{RotD50}, which is denoted:

$$\nu(\phi) = \frac{Sa(\phi)}{Sa_{\text{RotD50}}} = \frac{Sd(\phi)}{Sd_{\text{RotD50}}} \tag{2}$$

The ν ratios of the same 100 example ground motions are presented in Figure 2b. The particular case of $\nu(0°) = Sa_{\text{RotD100}}/Sa_{\text{RotD50}}$ has been studied previously [10,11] and its lower and upper bounds are 1 and $\sqrt{2}$, respectively [2]. The lower and upper bounds of ν for other rotation angles are significantly more complicated to derive, and hence their derivation is presented

in Appendix A. Again, a significant record-to-record variability exists on $\nu(\phi)$ with several records having ratios close to the upper bound for rotation angles smaller than 30°.

3 | PROBABILISTIC CHARACTERIZATION OF DIRECTIONALITY

The directionality of earthquake ground motion intensities is studied here using a subset of the NGA-West2 database, which contains ground motion records from shallow crustal earthquakes in active tectonic regimes worldwide[14]. The records were selected using the following criteria: (1) originated from earthquakes of magnitude greater than or equal to 5; (2) recorded in NEHRP site classes B, C, and D; and (3) have reasonably free-field conditions according to the criteria used by Boore et al.[3]. This resulted in 5,065 pairs of horizontal ground motions, which were used to compute the $\eta(\phi)$ and $\nu(\phi)$ ratios defined in the previous section for rotation angles varying from -90° to 90° every 0.5°. Both ratios were computed using spectral ordinates at 21 periods ranging from 0.01 to 10 s, which correspond to those used to define the multi-period design response spectrum in the latest NEHRP Recommended Seismic Provisions for New Buildings and Other Structures[15]. In total, a little more than thirty-eight million η and ν ratios were computed. At each period, the statistics were computed for the natural logarithm of the ratios because GMMs usually assume that spectral accelerations follow a lognormal probability distribution.

The geometric means of the ratios, μ_η and μ_ν, are presented in Figure 3 for five different periods, and are related to the mean of the logarithmic ratios by an exponential:

$$\mu_\eta(\phi) = \exp(\mathrm{E}\left[\ln \eta(\phi)\right]) \tag{3}$$

where $E[\cdot]$ represents the expectation function. As expected, the geometric means of both ratios monotonically decrease as the orientations separate from the major response axis. Moreover, the rate at which the ratios decrease is higher as the period of vibration increases, indicating that spectral ordinates become, on average, more polarized as the period of vibration increases and that significantly larger polarizations occur for long periods oscillators than those found by Hong and Goda[13] for the 1.0 s oscillators. In particular, for periods longer than 5 s, the intensity along the major response axis is, on average, approximately twice as large as the intensity in the perpendicular direction. Nonlinear regression analyses were conducted by using the following functional form in order to develop a model to estimate the geometric mean:

$$\hat{\mu}(\phi) = C_1 + C_2 e^{-C_3 \phi^2} \tag{4}$$

where ϕ is the angle from the major response axis (in radians) and coefficients C_1, C_2, and C_3 were obtained independently for each period of vibration and for both ratios of interest (i.e., η and ν) by solving a nonlinear least-squares problem using the Levenberg–Marquardt algorithm[16]. Coefficients C_1, C_2, and C_3 are given in Tables B1 and B2 of Appendix B to estimate the geometric mean of η and ν, respectively. The resulting regression models are presented in Figure 3 and compared to the empirical data, showing that both models fit both ratios very well for all combinations of period and rotation angles, ϕ. Geometric means of intensities equal to the RotD50 intensity occur at rotation angles between 39° and 43° for periods between 0.1 and 10 s.

The next statistic that was studied was the standard deviation of the logarithmic ratios, $\sigma_{\ln\eta}$ and $\sigma_{\ln\nu}$, which are presented in Figure 4. Because, by definition, η ratios are spectral intensities normalized by the maximum intensity, then $\eta(0°) = 1$ for all ground motions, and therefore the standard deviation of $\ln\eta$ is zero at the major response axis (i.e., $\phi = 0°$). As the angle of rotation with respect to the major response axis increases, $\sigma_{\ln\eta}$ increases monotonically, which is also observed in Figure 2a. In contrast, $\sigma_{\ln\nu}$ remains relatively stable at roughly 0.08 up to a rotation angle of approximately $\phi = 20°$, then slightly decreases, and then increases monotonically for rotation angles larger than approximately $\phi = 45°$. Thus, the smallest record-to-record variability of ν occurs at a rotation angle of approximately $\phi = 45°$. Moreover, in both cases, the standard deviation is relatively period insensitive up to an angle of approximately $\phi = 60°$, from which the long period oscillators start to have a higher standard deviation.

Regression models were also fitted to $\sigma_{\ln\eta}$ and $\sigma_{\ln\nu}$ with the following function form:

$$\hat{\sigma}_{\ln}(\phi) = \frac{C_4 + C_5\phi^3 + C_6\phi^4}{1 + C_7\phi^3 + C_8\phi^4} \tag{5}$$

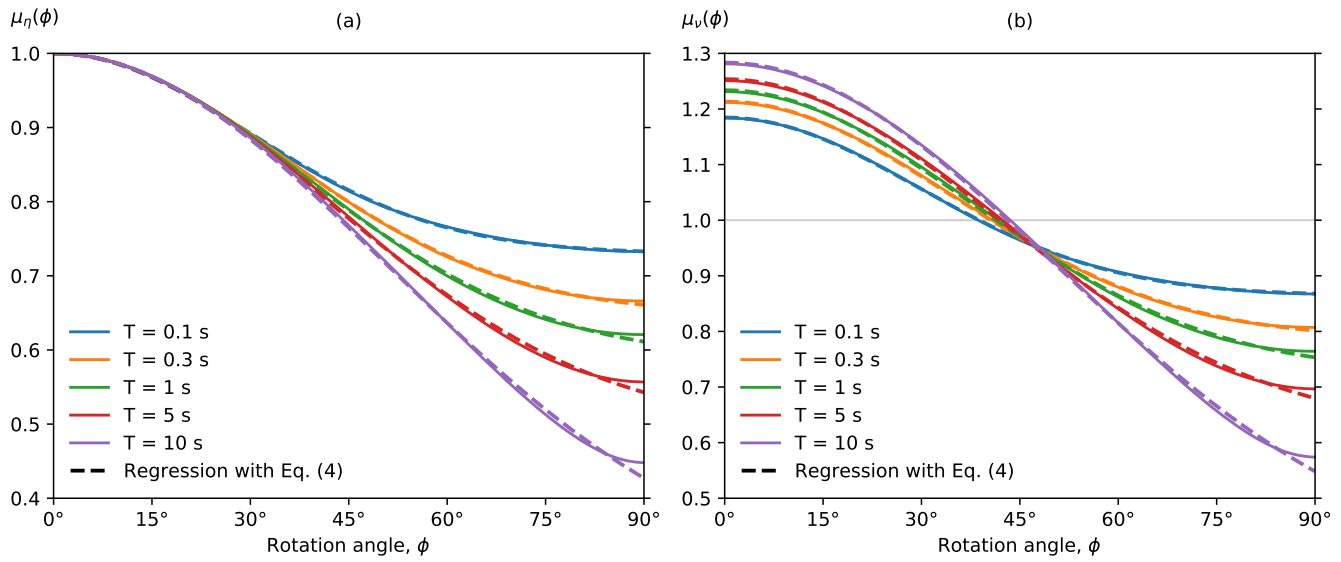

FIGURE 3 Geometric means of (a) η and (b) ν. Solid lines represent empirical data and dashed lines represent estimates obtained with the regression model using Equation 4.

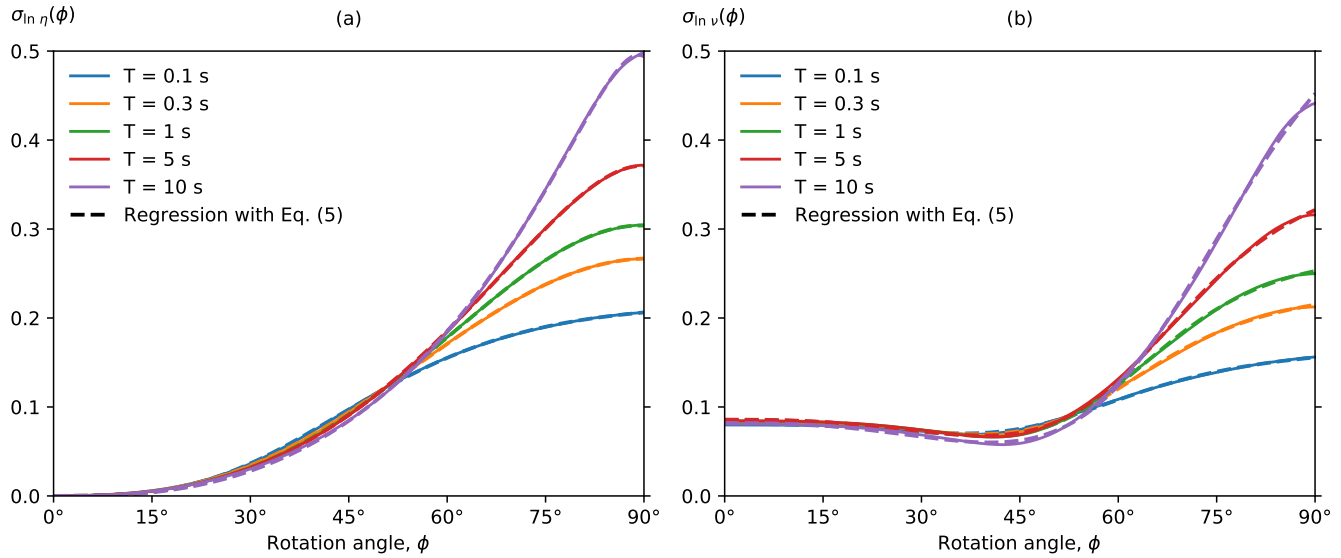

FIGURE 4 Standard deviation of (a) $\ln\eta$ and (b) $\ln\nu$. Solid lines represent empirical data and dashed lines represent estimates obtained with the regression model using Equation 5.

where ϕ is in radians and coefficients C_4, C_5, C_6, C_7, and C_8 were again estimated independently for each period of vibration. The resulting models are compared to the empirical results in Figure 4 showing that thy fit the data very well.

The final statistical measure that was studied was the Pearson correlation coefficient between the logarithm of the ratio at two different angles ϕ and ψ:

$$\rho_{\ln\eta}(\phi,\psi) = \frac{\mathrm{Cov}(\ln\eta(\phi), \ln\eta(\psi))}{\sigma_{\ln\eta}(\phi)\sigma_{\ln\eta}(\psi)} \tag{6}$$

where Cov(·, ·) is the covariance between two random variables. Figure 5 shows the correlations of both ratios for different combinations of both angles for oscillators with a period of vibration of 1 s. Both correlations are close to one if the angles are close to each other and decrease as the rotation angles separate. However, $\rho_{\ln \eta}$ remains always positive whereas $\rho_{\ln \nu}$ becomes negative when the angles are very separated. Note that $\rho_{\ln \eta}$ is undefined for $\psi = 0°$ and $\psi = 180°$ because $\ln \eta(0°)$ and $\ln \eta(180°)$ have no uncertainty (they are always 0), and hence are not presented in Figure 5a.

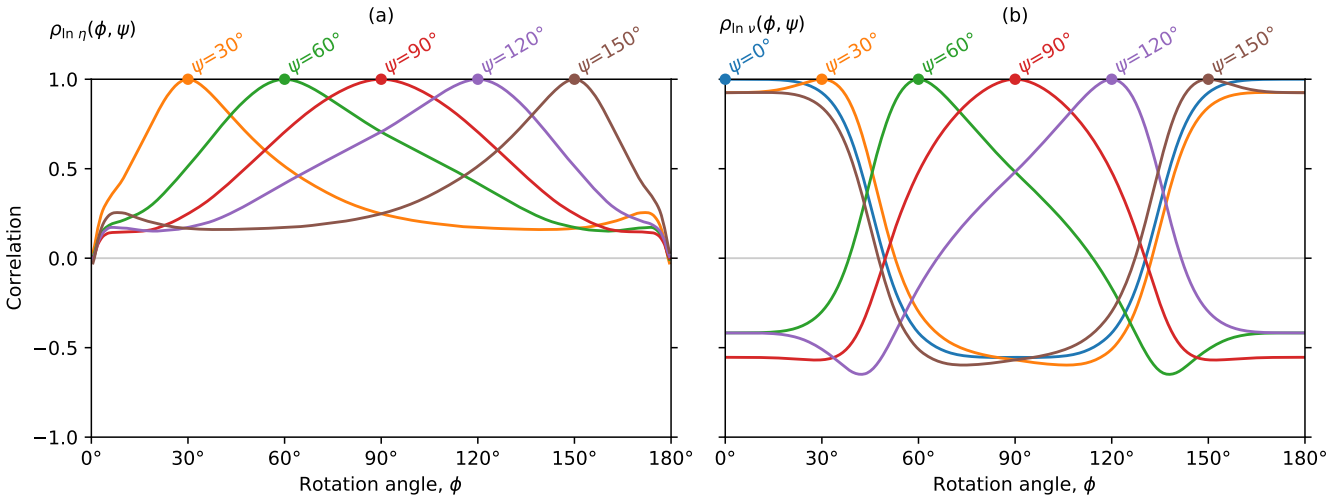

FIGURE 5 Correlations of (a) $\ln \eta$ and (b) $\ln \nu$ at two rotation angles ϕ and ψ for a period of vibration of 1 s.

A relevant special case of the correlations of Equation (6) is when angles ϕ and ψ are separated by 90° (i.e., the orientations are orthogonal to each other), which is usually the case for the principal axes of buildings and many other types of structures. These correlations are shown in Figure 6 for different periods, which shows that both are relatively constant throughout the range ϕ. The values of $\rho_{\ln \eta}$ for orthogonal orientations tend to increase slightly as the period increases and are always relatively low, with the correlation coefficient usually lower than 0.2. Thus, neglecting these correlations could be a reasonable simplifying assumption. However, correlation $\rho_{\ln \nu}$ is more significant than $\rho_{\ln \eta}$ for orthogonal orientations, with its values always negative and its mean value ranging from approximately -0.45 for a period of 0.1 s to -0.64 for 10 s. Given the relatively stable value of $\rho_{\ln \nu}$ throughout the range of ϕ, using a constant value that depends on period is a reasonable assumption. If more accurate estimations are required, a regression model with the following functional form can be used:

$$\hat{\rho}_{\ln \nu}(\phi, \phi + \pi/2) = C_9 + C_{10} e^{-C_{11}(\phi - \pi/4)^2} \tag{7}$$

Figure 6b compares the correlation coefficients of $\ln \nu$ estimated with Equation (7) to those of the data, showing that they fit very well. Note that the correlations from Equation (7) are only for orthogonal orientation pairs and that no model is presented for a generic pair of orientations due to its lower practical applicability since the great majority of structures have principal axes that are orthogonal to each other. The coefficients of all fitted regression models (C_1-C_{11}) are presented in Tables B1 and B2 of Appendix B and in the Electronic Supplement of this article.

For some applications, such as the simulation of realizations of spectral ordinates in different orientations, the full distribution of η and ν is necessary. Figure 7 shows the empirical distributions of the ratios for two vibration periods (0.1 and 1 s) at different angles ϕ. All ratios have upper and lower bounds that depend on ϕ, as shown in Figure 2. A four-parameter beta distribution was fitted to each combination of period and ϕ using maximum likelihood estimation. The probability density functions of these fitted distributions are compared to the empirical distribution in Figure 7, showing a relatively good fit. Note that for $\eta(0°)$ the probability density function becomes a Dirac delta function because by definition η is always 1 at $\phi = 0°$. The parameters of the fitted beta distributions are presented in the Electronic Supplement of this article.

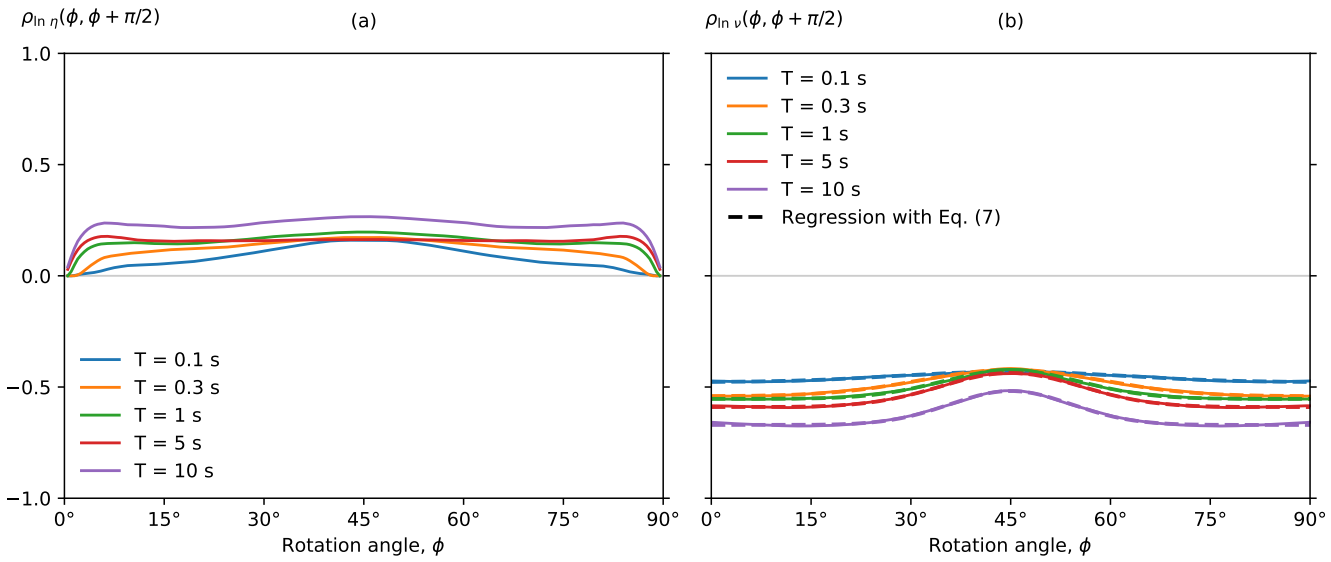

FIGURE 6 Correlations of (a) $\ln \eta$ and (b) $\ln \nu$ between two orthogonal horizontal orientations. Solid lines represent empirical data and dashed lines in (b) represent estimates obtained with the regression model using Equation 7.

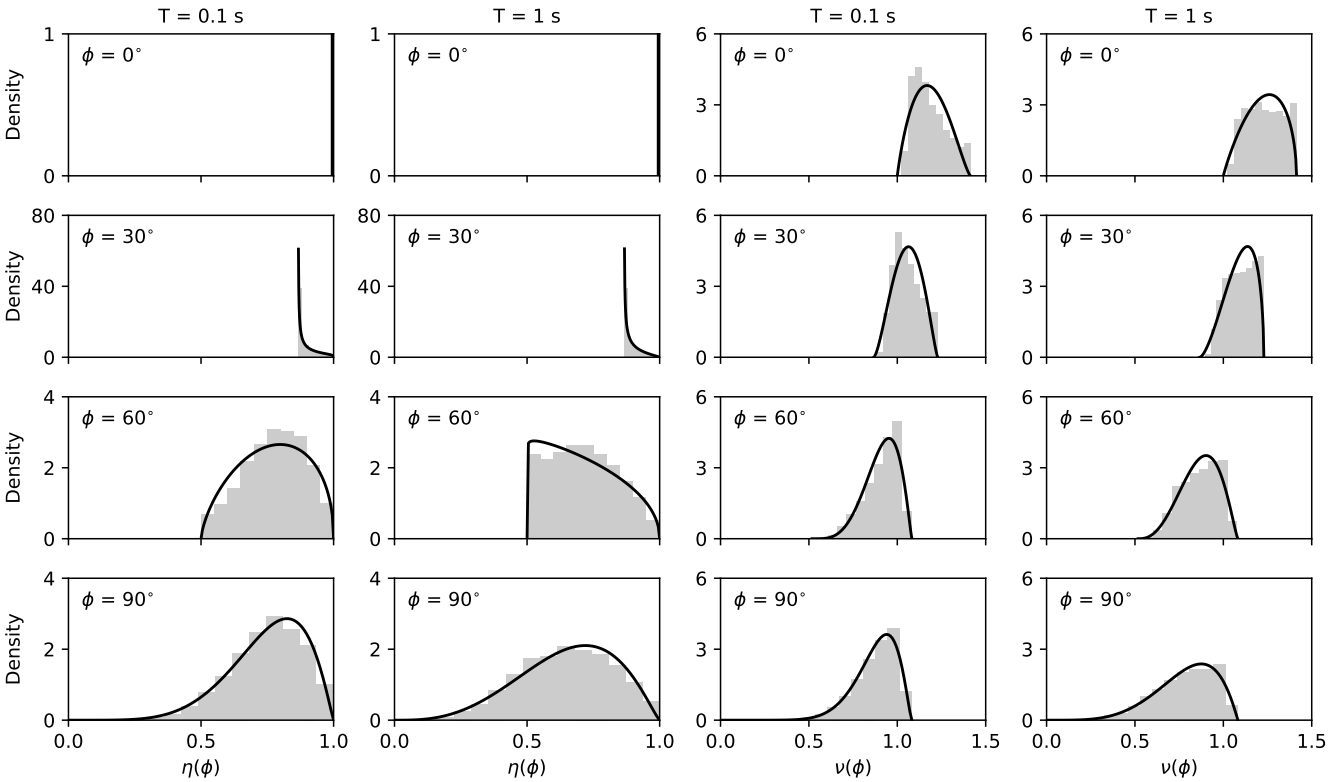

FIGURE 7 Empirical and fitted probability distributions of η and ν at periods of 0.1 and 1.0 s for four different angles ϕ.

4 | NOVELTY AND SIGNIFICANCE OF RESULTS

Previous works that studied at least one of the two ratios presented here are shown in Table 1. Although values for the geometric mean of η and ν have already been presented by Hong and Goda[13] and Shahi and Baker[10], respectively, the rest of the statistics, that is, the standard deviations, correlations, and probability distribution, have not been studied previously, except for a few cases. One of these cases is when $\phi = 0°$, which leads to $\nu = Sa_{\text{RotD100}}/Sa_{\text{RotD50}}$, whose logarithmic standard deviation has been computed previously[10,11]. The other special case is for the η ratio when $\phi = 90°$, whose probability distribution was fitted by Hong and Goda[13] at six periods between 0.1 and 3 s. The results and models presented in this work extend those of previous studies and thus have a wider range of applicability.

TABLE 1 Previous works that studied the η and ν ratios.

Ratio	Property	Hong and Goda[13]	Shahi and Baker[10]	Boore and Kishida[11]	This study
$\eta(\phi)$	$\mu_{\eta}(\phi)$	✓	-	-	✓
	$\sigma_{\ln\eta}(\phi)$	-	-	-	✓
	$\rho_{\ln\eta}$	-	-	-	✓
	Distribution	only $\phi = 90°$	-	-	✓
	Bounds	✓	-	-	✓
$\nu(\phi)$	$\mu_{\nu}(\phi)$	-	✓	only $\phi = 0°$	✓
	$\sigma_{\ln\nu}(\phi)$	-	only $\phi = 0°$	only $\phi = 0°$	✓
	$\rho_{\ln\nu}$	-	-	-	✓
	Distribution	-	-	-	✓
	Bounds	-	only $\phi = 0°$	-	✓

The detailed probabilistic characterization of the orientation dependence of horizontal response spectra provided by this study could be used in several future applications. For example, the statistics of the ν ratios could be used to simulate earthquake response spectra at one or more orientations at the same site. These orientations could represent, for example, the two horizontal principal axes of buildings, which are usually orthogonal. For a given earthquake scenario, the response spectral ordinate could be computed by following these steps:

1. Compute Sa_{RotD50} using one or more of the several available GMMs that consider RotD50[3].
2. Define the orientation where Sa_{RotD100} occurs (i.e., the major response axis). Previous studies suggest that at sites that are far away from the fault, the orientation of the major response axis can be considered to be uniformly distributed, whereas at sites close to the rupture the major response axis tends to be closer to the fault normal orientation[10].
3. Compute the angular differences between the major response axis and the orientations of interest (e.g., the two principal axes of a structure).
4. Compute the response spectra at the orientations of interest. One option to achieve this is by modifying the logarithmic mean and possibly also the logarithmic standard deviation obtained from the GMM using the expressions for the logarithmic mean and standard deviation of $\nu(\phi)$. Another option is the sample Sa_{RotD50} from a lognormal probability distribution using the GMM and then multiply them by $\nu(\phi)$ ratios from the fitted distributions to obtain a realization of $Sa(\phi)$.

An interesting application of this procedure is regional risk assessment of buildings, where the orientations of the major response axes at sites that are close to each other tend to be strongly correlated, especially at long periods[17]. Moreover, the orientation of the principal axes of different buildings within a city also tend to be very similar because of regularities in street network layouts. If all orientations of the maximum ground motion intensity are assumed to be equally likely, and therefore changing from earthquake to earthquake with respect to the orientation of the principal axes of the buildings, the expected annual sum of losses from all buildings should not be affected by these correlations because it corresponds to the sum of the expected annual losses of the building, which are computed independently without the use of correlation. However, neglecting these correlations

could lead to an underestimation of losses in individual events as well as of rare losses with small rates of occurrence (i.e., high return periods) and an overestimation of frequent losses, similarly to what occurs when neglecting the spatial correlation of ground motion intensities [18].

5 | CONCLUSIONS

The variation of response spectral ordinates with changes in orientation within the horizontal plane, typically referred to as ground motion directionality, is characterized probabilistically and a new model to explicitly account for directionality is developed. The study of directionality of earthquake spectral responses is based on the use of a large database of ground motion recordings. Two metrics are used to characterize ground motion directionality in which ratios between spectral ordinates within the horizontal plane and normalized by their median (RotD50) or maximum (RotD100) values for all orientations, which are commonly used orientation independent intensity measures. Several statistical properties of these ratios were studied, namely, their geometric mean, logarithmic standard deviation, and correlation. Nonlinear regression models were fitted to each of these statistics to simplify their future use. Furthermore, probability distributions were fitted to the studied ratios, which could be used if full probabilistic characterization of directionality is required. These probabilistic characterizations can be used in the future to simulate orientation-dependent ground motion intensities. One possible application of these results is for seismic risk assessment of buildings, where current methods are based on orientation independent intensity measure (e.g., RotD50) and therefore do not take into account the orientation of the principal axes of buildings.

ACKNOWLEDGMENTS

The authors would like to acknowledge the National Agency for Research and Development (ANID) / Doctorado Becas Chile / 2019-72200307 and the Nancy Grant Chamberlain Fellowship at Stanford University for sponsoring the doctoral studies of the first author. Additionaly, the authors would like to thank Professor Pablo Heresi, now at the Federico Santa María Technical University in Chile, for his comments on initial aspects of this research.

DATA AVAILABILITY STATEMENT

The ground motion records used in this study were downloaded from the NGA-West2 database developed by the Pacific Earthquake Engineering Research Center (https://ngawest2.berkeley.edu/spectras/new, last accessed April 2020). The coefficients of the nonlinear regression models and the parameters of the probability distributions fitted in this study are provided in CSV files in an Electronic Supplement.

References

1. Boore DM, Watson-Lamprey J, Abrahamson NA. Orientation-independent measures of ground motion. *Bulletin of the Seismological Society of America* 2006; 96(4A): 1502–1511.

2. Boore DM. Orientation-independent, nongeometric-mean measures of seismic intensity from two horizontal components of motion. *Bulletin of the Seismological Society of America* 2010; 100(4): 1830–1835.

3. Boore DM, Stewart JP, Seyhan E, Atkinson GM. NGA-West2 equations for predicting PGA, PGV, and 5% damped PSA for shallow crustal earthquakes. *Earthquake Spectra* 2014; 30(3): 1057–1085.

4. American Society of Civil Engineers . *Minimum design loads and associated criteria for buildings and other structures, ASCE/SEI 7-16*. Reston, VA: American Society of Civil Engineers . 2016.

5. Huang YN, Whittaker AS, Luco N. Maximum spectral demands in the near-fault region. *Earthquake Spectra* 2008; 24(1): 319–341.

6. Poulos A, Miranda E. Proposal of orientation-independent measure of intensity for earthquake-resistant design. *Earthquake Spectra* 2022; 38(1): 235–253.
7. Poulos A, Miranda E, Baker JW. Evaluation of earthquake response spectra directionality using stochastic simulations. *Bulletin of the Seismological Society of America* 2022; 112(1): 307–315.
8. Beyer K, Bommer JJ. Relationships between median values and between aleatory variabilities for different definitions of the horizontal component of motion. *Bulletin of the Seismological Society of America* 2006; 96(4A): 1512–1522.
9. Watson-Lamprey JA, Boore DM. Beyond Sa_{GMRotI}: Conversion to Sa_{Arb}, Sa_{SN}, and Sa_{MaxRot}. *Bulletin of the Seismological Society of America* 2007; 97(5): 1511–1524.
10. Shahi SK, Baker JW. NGA-West2 models for ground motion directionality. *Earthquake Spectra* 2014; 30(3): 1285–1300.
11. Boore DM, Kishida T. Relations between some horizontal-component ground-motion intensity measures used in practice. *Bulletin of the Seismological Society of America* 2017; 107(1): 334–343.
12. Poulos A, Miranda E. Relations between MaxRotD50 and some horizontal components of ground-motion intensity used in practice. *Bulletin of the Seismological Society of America* 2021; 111(4): 2167–2176.
13. Hong HP, Goda K. Orientation-dependent ground-motion measure for seismic-hazard assessment. *Bulletin of the Seismological Society of America* 2007; 97(5): 1525–1538.
14. Ancheta TD, Darragh RB, Stewart JP, et al. NGA-West2 database. *Earthquake Spectra* 2014; 30(3): 989–1005.
15. Building Seismic Safety Council . *NEHRP recommended seismic provisions for new buildings and other structures, volume I: part 1 provisions, part 2 commentary, FEMA P-2082-1*. Washington, D.C.: Federal Emergency Management Agency . 2020.
16. Moré JJ. The Levenberg-Marquardt algorithm: implementation and theory. In: Watson GA., ed. *Numerical Analysis*. Lecture Notes in Mathematics. Springer. 1978 (pp. 105–116).
17. Filippitzis F, Kohler MD, Heaton TH, et al. Ground motions in urban Los Angeles from the 2019 Ridgecrest earthquake sequence. *Earthquake Spectra* 2021; 37(4): 2493–2522.
18. Park J, Bazzurro P, Baker JW. Modeling spatial correlation of ground motion intensity measures for regional seismic hazard and portfolio loss estimation. In: Tenth International Conference on Application of Statistics and Probability in Civil Engineering. ; 2007; Tokyo, Japan.

How to cite this article: Poulos A, Miranda E. Probabilistic characterization of the directionality of horizontal earthquake response spectra. *Earthquake Engng Struct Dyn*. 2022;51:2077-2090. doi:10.1002/eqe.3654

APPENDIX

A DERIVATION OF THE UPPER AND LOWER BOUNDS OF $\nu(\phi)$

A convenient way to derive the bounds of the ν ratios is to use the η ratios because their upper and lower bounds are 1 and $\cos(\phi)$, respectively. Figure A1 shows these upper and lower bounds of η in dashed lines along with a possible variations of η ratios within the range of non-redundant angles $\phi \in [0°, 180°]$. The objective is to find variations of η that minimize and maximize ν at each value of ϕ. Any possible variation must be between the bounds of η, i.e. $|\cos(\phi)| \leq \eta(\phi) \leq 1$.

We start by deriving the lower bound of ν. Let y be the value of η at a given angle of interest ϕ where we want to derive the lower bound. The value of y from the η distribution that leads to the lower bound is unknown, therefore, here we consider the minimum value of ν for all possible values of y and then take the minimum:

$$\nu_{\min}(\phi) = \min_{y \in [\cos(\phi), 1]} \frac{y}{\eta_{\text{RotD50}}(\phi, y)} \tag{A1}$$

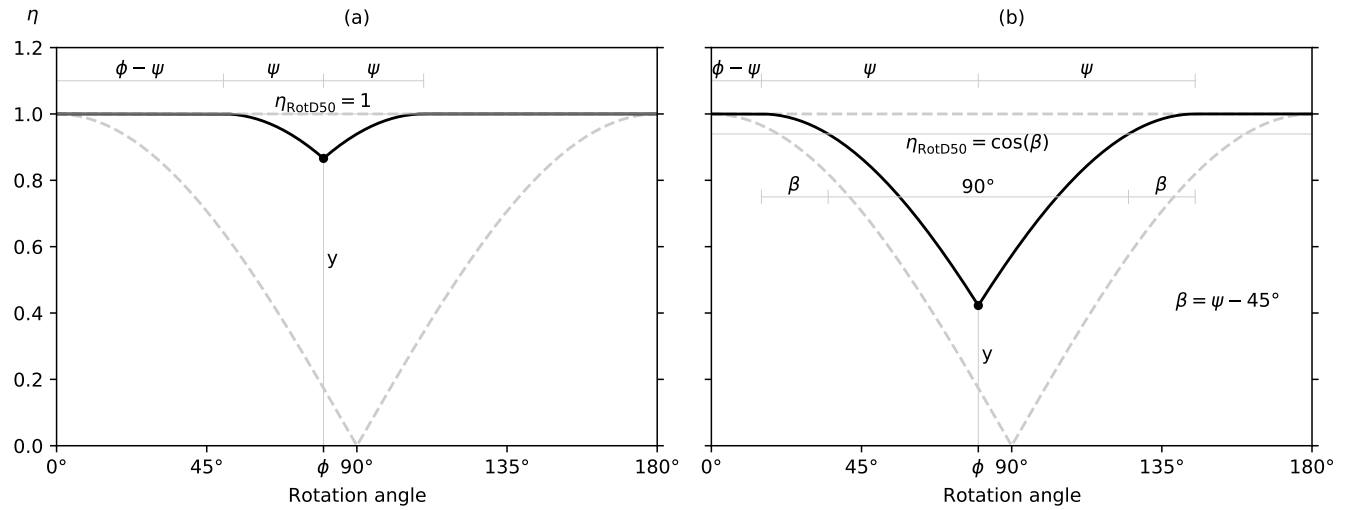

FIGURE A1 Variation of η ratios that maximize η_{RotD50} for a given value of ϕ and y, for cases when (a) $\psi < 45°$ and (b) $\psi > 45°$.

where η_{RotD50} is the median value of the η distribution (i.e., $\eta_{\text{RotD50}} = Sa_{\text{RotD50}}/Sa_{\text{RotD100}}$). Since the fixed value of y corresponds to the numerator of the ratio that is being minimized, the minimum value of the ratio occurs when the denominator, $\eta_{\text{RotD50}}(\phi, y)$, is maximized. To accomplish this, the variation of η takes its highest possible value at each rotation angle, given that $\eta(\phi) = y$, as seen in Figure A1. To simplify the expressions, we make the change of variable $y = \cos(\psi)$, leading to:

$$\nu_{\text{min}}(\phi) = \min_{\psi \in [0,\phi]} \frac{\cos(\psi)}{\eta_{\text{RotD50}}(\phi, \psi)} \tag{A2}$$

The value of η_{RotD50} can then be computed in terms of ψ:

$$\eta_{\text{RotD50}}(\phi, \psi) = \begin{cases} 1 & \text{if } \psi \leq 45° \\ \cos(\psi - 45°) & \text{if } \psi > 45° \end{cases} \tag{A3}$$

Note that η_{RotD50} does not depend on ϕ, only on ψ, and that its value is 1 for $\psi < 45°$ because more than half of the rotation angles have $\eta = 1$. Solving the minimization problem defined by Equations (A2) and (A3) results in:

$$\nu_{\text{min}}(\phi) = \begin{cases} \cos(\phi) & \text{if } \phi \leq 45° \\ \dfrac{\cos(\phi)}{\cos(\phi - 45°)} & \text{if } \phi > 45° \end{cases} \tag{A4}$$

where the value of ψ that minimizes the ratio is always equal to ϕ. In other words, the variation of η that minimizes ν always has $y = \cos(\phi)$.

The upper bound of ν can be found in a similar manner, but now by maximizing the ratio:

$$\nu_{\text{max}}(\phi) = \max_{\psi \in [0,\phi]} \frac{\cos(\psi)}{\eta_{\text{RotD50}}(\phi, \psi)} \tag{A5}$$

The variation of η distribution that minimizes the denominator, η_{RotD50}, for given values of ϕ and y (or ψ) is shown in Figure A2. An ideal case that generates this variation is a ground motion that is fully polarized in the 0° orientation, then stops until the SDOF system finishes oscillating, and finally has the same fully polarized motion in the $(\phi - \psi)$ orientation. Depending on the values of ϕ and ψ there can be two cases, one where η_{RotD50} is below the left local minimum of η (Case 1) and another where η_{RotD50} is above both local minima (Case 2). The cases that are associated with each combination of ϕ and ψ are presented in Figure A3a, with the limit between these two cases occurring when $\phi - \psi = 45°$.

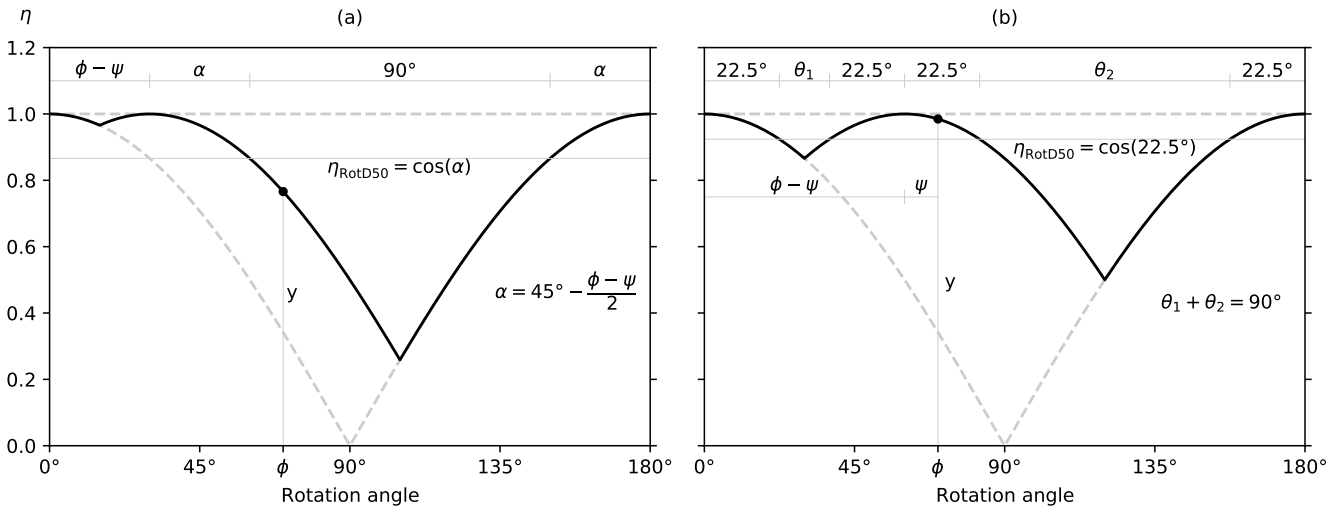

FIGURE A2 Variation of η ratios that minimize η_{RotD50} for a given value of ϕ and y, for the case when (a) $\phi - \psi < 45°$ and (b) $\phi - \psi > 45°$.

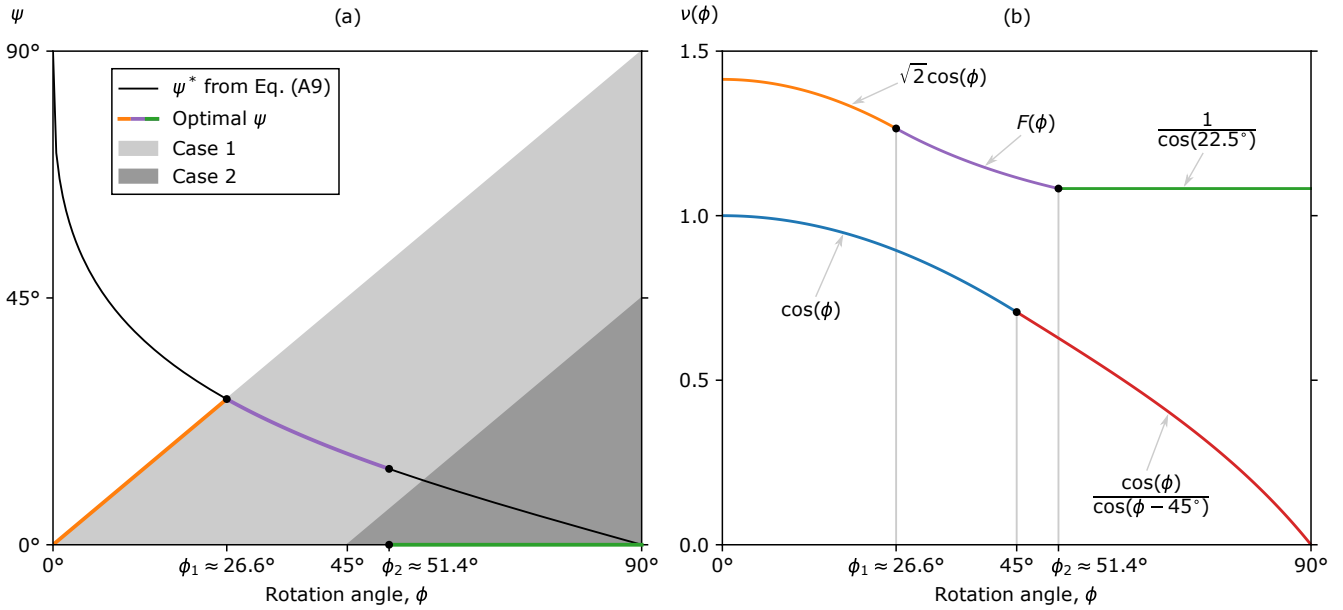

FIGURE A3 (a) Values of ψ that minimize ν for each for each rotation angle ϕ. (b) Functions that define the minimum and maximum value of ν as a function of ϕ.

Case 1 occurs when $\phi - \psi < 45°$ and the computation of η_{RotD50} is shown in Figure A2a. The value of η_{RotD50} in this case is:

$$\eta^{(1)}_{\text{RotD50}}(\phi, \psi) = \cos\left(45° - \frac{(\phi - \psi)}{2}\right) \tag{A6}$$

Thus, the ν ratio for this case is given by:

$$\nu^{(1)}(\phi, \psi) = \frac{\cos(\psi)}{\cos\left(45° - (\phi - \psi)/2\right)} \tag{A7}$$

To obtain the value of ψ that maximizes $\nu^{(1)}$ (ψ^*), we can take the partial derivative of $\nu^{(1)}$ with respect to ψ as follows:

$$\frac{\partial}{\partial\psi}\left(\nu^{(1)}(\phi,\psi)\right) = \frac{-\sin(\psi)\cos\left(45° - (\phi-\psi)/2\right) - \cos(\psi)\sin(45° - (\phi-\psi)/2)}{\cos^2\left(45° - (\phi-\psi)/2\right)} \tag{A8}$$

and then obtain the value of ψ that makes the derivative equal to zero, which is given by:

$$\psi^* = 2\cos^{-1}\left(\sqrt{\frac{1}{2} - \sin\left(\frac{\phi}{2}\right)\cos\left(\frac{\phi}{2}\right) + \sin^{5/3}\left(\frac{\phi}{2}\right)\cos^{1/3}\left(\frac{\phi}{2}\right) + \sin^{1/3}\left(\frac{\phi}{2}\right)\cos^{5/3}\left(\frac{\phi}{2}\right)}\right) \tag{A9}$$

If a simpler equation is desired for ψ^*, a very good fit is achieved with the following second degree polynomial:

$$\psi^* \approx 0.276\phi^2 - 0.883\phi + 0.812 \tag{A10}$$

where both ϕ and ψ^* are in radians. Using any of these expressions in Equation (A7):

$$F(\phi) = \frac{\cos(\psi^*)}{\cos\left(45° - (\phi-\psi^*)/2\right)} \tag{A11}$$

Figure A3a shows the values of ψ^* as a function of ϕ. At angles lower than $\phi_1 \approx 26.6°$, ψ^* is larger than the upper bound of ψ from the optimization problem (ϕ). Thus, the value of ψ that maximizes $\nu^{(1)}$ is $\psi = \phi$, and the upper bound of the ν ratio is:

$$\nu_{\max}(\phi) = \nu^{(1)}(\phi,\phi) = \frac{\cos(\phi)}{\cos(45°)} = \sqrt{2}\cos(\phi), \qquad \phi \in [0°, \phi_1] \tag{A12}$$

At angles higher than ϕ_1, ψ^* is within the bounds of the optimization problem. Thus, the upper bound of the ν ratio is given by:

$$\nu_{\max}(\phi) = F(\phi), \qquad \phi \in [\phi_1, \phi_2] \tag{A13}$$

at least up to an angle ϕ_2, which is obtained by comparing this result with the one from Case 2.

Case 2 occurs when $\phi - \psi > 45°$ and the computation of η_{RotD50} is shown in Figure A2b. In this case, the value of η_{RotD50} remains constant at:

$$\eta^{(2)}_{\text{RotD50}}(\phi,\psi) = \cos(22.5°) \tag{A14}$$

Thus, the ν ratio for this case is:

$$\nu^{(2)}(\phi,\psi) = \frac{\cos(\psi)}{\cos(22.5°)} \tag{A15}$$

Since $\cos(\psi)$ is a monotonically decreasing function in the range of interest ($\psi \in [0°, 90°]$), the maximum occurs at $\psi = 0°$ and has a value of:

$$\nu^{(2)}_{\max}(\phi) = \frac{1}{\cos(22.5°)} \tag{A16}$$

This solution is greater than $F(\phi)$ for angle $\phi > \phi_2 \approx 51.4°$, and therefore corresponds to the upper bound of the ν ratio within this range, which is given by:

$$\nu_{\max}(\phi) = \frac{1}{\cos(22.5°)}, \qquad \phi \in [\phi_2, 90°] \tag{A17}$$

Putting all together, the upper bound of the ν ratio is given by:

$$\nu_{\max}(\phi) = \begin{cases} \sqrt{2}\cos(\phi) & \text{if } 0° \leq \phi \leq \phi_1 \\ F(\phi) & \text{if } \phi_1 < \phi < \phi_2 \\ 1/\cos(22.5°) & \text{if } \phi_2 \leq \phi \leq 90° \end{cases} \tag{A18}$$

Figure A3b summarizes the upper and lower bound of the ν ratio derived here.

B COEFFICIENTS OF THE FITTED REGRESSION MODELS

TABLE B1 Coefficients of the regression models for η.

Period (s)	C_1	C_2	C_3	C_4	C_5	C_6	C_7	C_8
0.010	0.720	0.280	1.824	0	0.243	0.057	0.433	0.552
0.020	0.722	0.278	1.837	0	0.244	0.063	0.468	0.563
0.030	0.724	0.276	1.858	0	0.256	0.045	0.514	0.495
0.050	0.730	0.270	1.911	0	0.232	0.100	0.566	0.676
0.075	0.733	0.267	1.908	0	0.239	0.091	0.620	0.636
0.100	0.730	0.270	1.868	0	0.254	0.067	0.685	0.510
0.150	0.705	0.295	1.666	0	0.299	-0.057	0.501	0.104
0.200	0.682	0.318	1.537	0	0.303	-0.092	0.319	0.043
0.250	0.664	0.336	1.426	0	0.314	-0.112	0.336	-0.042
0.300	0.649	0.351	1.373	0	0.314	-0.135	0.172	-0.030
0.400	0.628	0.372	1.293	0	0.305	-0.130	0.096	0.001
0.500	0.617	0.383	1.252	0	0.299	-0.134	-0.008	0.035
0.750	0.597	0.403	1.181	0	0.297	-0.139	-0.063	0.045
1.000	0.588	0.412	1.168	0	0.289	-0.133	-0.100	0.068
1.500	0.572	0.428	1.118	0	0.298	-0.146	-0.102	0.042
2.000	0.557	0.443	1.076	0	0.293	-0.143	-0.152	0.068
3.000	0.543	0.457	1.046	0	0.300	-0.151	-0.152	0.054
4.000	0.519	0.481	1.006	0	0.282	-0.138	-0.203	0.086
5.000	0.492	0.508	0.937	0	0.290	-0.153	-0.264	0.089
7.500	0.342	0.658	0.705	0	0.273	-0.160	-0.464	0.161
10.000	0.278	0.722	0.638	0	0.266	-0.156	-0.523	0.195

TABLE B2 Coefficients of the regression models for ν.

Period (s)	C_1	C_2	C_3	C_4	C_5	C_6	C_7	C_8	C_9	C_{10}	C_{11}
0.010	0.858	0.335	1.842	0.084	-0.335	0.366	-2.057	2.178	-0.469	0.056	9.292
0.020	0.860	0.333	1.855	0.084	-0.335	0.369	-2.056	2.203	-0.468	0.046	6.867
0.030	0.862	0.329	1.875	0.083	-0.316	0.350	-1.976	2.116	-0.478	0.055	5.929
0.050	0.867	0.321	1.927	0.083	-0.317	0.361	-1.921	2.179	-0.467	0.052	6.981
0.075	0.868	0.317	1.918	0.082	-0.303	0.351	-1.865	2.147	-0.487	0.064	2.870
0.100	0.865	0.320	1.877	0.081	-0.283	0.341	-1.606	1.977	-0.478	0.048	5.978
0.150	0.842	0.352	1.671	0.082	-0.291	0.320	-1.679	1.751	-0.501	0.061	5.851
0.200	0.821	0.383	1.548	0.084	-0.310	0.328	-1.692	1.665	-0.512	0.074	10.330
0.250	0.802	0.406	1.434	0.084	-0.296	0.321	-1.406	1.436	-0.518	0.063	9.365
0.300	0.787	0.426	1.385	0.084	-0.298	0.317	-1.491	1.441	-0.541	0.119	8.970
0.400	0.767	0.455	1.308	0.086	-0.306	0.320	-1.446	1.362	-0.540	0.116	13.316
0.500	0.756	0.468	1.268	0.086	-0.314	0.319	-1.526	1.369	-0.567	0.153	15.430
0.750	0.734	0.496	1.198	0.085	-0.313	0.320	-1.508	1.349	-0.562	0.130	12.225
1.000	0.726	0.508	1.185	0.085	-0.312	0.318	-1.464	1.295	-0.553	0.128	15.103
1.500	0.708	0.530	1.136	0.085	-0.306	0.315	-1.398	1.242	-0.557	0.121	13.127
2.000	0.692	0.548	1.093	0.085	-0.311	0.320	-1.398	1.235	-0.576	0.156	11.671
3.000	0.677	0.567	1.062	0.086	-0.316	0.325	-1.359	1.198	-0.562	0.084	5.956
4.000	0.652	0.601	1.025	0.085	-0.305	0.317	-1.225	1.083	-0.565	0.122	11.439
5.000	0.619	0.634	0.952	0.086	-0.297	0.307	-1.097	0.946	-0.590	0.153	14.799
7.500	0.440	0.836	0.714	0.083	-0.297	0.309	-0.730	0.616	-0.646	0.203	17.151
10.000	0.361	0.922	0.647	0.082	-0.296	0.302	-0.765	0.604	-0.671	0.153	19.527